

M³-VOS: Multi-Phase, Multi-Transition, and Multi-Scenery Video Object Segmentation

Zixuan Chen*

m13953842591@sjtu.edu.cn

Yejie Guo

gyj123@sjtu.edu.cn

Jiaxin Li*

li_jiaxin@sjtu.edu.cn

Liming Tan

spinningfever@sjtu.edu.cn

Junxuan Liang

whitefork@sjtu.edu.cn

Cewu Lu

lucewu@sjtu.edu.cn

Yong-Lu Li[†]

yonglu_li@sjtu.edu.cn

Shanghai Jiao Tong University

Abstract

Intelligent robots need to interact with diverse objects across various environments. The appearance and state of objects frequently undergo complex transformations depending on the object properties, e.g., phase transitions. However, in the vision community, segmenting dynamic objects with phase transitions is overlooked. In light of this, we introduce the concept of **phase** in segmentation, which categorizes real-world objects based on their visual characteristics and potential morphological and appearance changes. Then, we present a new benchmark, **Multi-Phase, Multi-Transition, and Multi-Scenery Video Object Segmentation (M³-VOS)**, to verify the ability of models to understand object phases, which consists of 479 high-resolution videos spanning over 10 distinct everyday scenarios. It provides dense instance mask annotations that capture both object phases and their transitions. We evaluate state-of-the-art methods on M³-VOS, yielding several key insights. Notably, current appearance-based approaches show significant room for improvement when handling objects with phase transitions. The inherent changes in disorder suggest that the predictive performance of the forward entropy-increasing process can be improved through a reverse entropy-reducing process. These findings lead us to propose ReVOS, a new plug-and-play model that improves its performance by reversal refinement. Our data and code will be publicly available at <https://zixuan-chen.github.io/M-cube-VOS.github.io/>.

1. Introduction

Object understanding is crucial, especially for Embodied AI. Lately, large-scale datasets and data-driven methods [6, 16] have advanced research in object understanding, shifting from traditional category recognition [13] to deeper levels of comprehension, such as identifying higher-level affordances [10] and attributes [11], which help establishing the concepts of objects in interactions with environment.

In the real world, intelligent robots need to interact with various objects in diverse ways, during which, objects exhibit a range of morphological and appearance changes influenced by their inherent characteristics, the nature of the environment, and the specific interactions occurring. Particularly, the **phase** characteristics of objects describe their intrinsic morphological features and change dynamics, making them an important component of object knowledge.

Objects with different phase characteristics exhibit distinct change features when subjected to the same interactions. For instance, placing solid coffee beans in a blender results in their transformation into a powdered form. In contrast, pouring milk into the blender causes it to splash and flow continuously during blending, potentially even leading to separation at the end. In addition to transformations **within** phase states, **cross**-state phase changes are common in the real world, endowing objects with properties they originally did not have. For example, dry ice rapidly sublimates, producing a lot of mist and water droplets will quickly frost at lower temperatures as Fig. 1. Therefore, a deep understanding of an object’s intrinsic phase characteristics and the properties of phase transition is crucial for robots to perceive the world, manipulate objects, and fulfill various complex functions according to human needs.

Despite efforts exploring the visual understanding of object change characteristics from various perspectives, such

*Equal contributions. [†]Corresponding author.

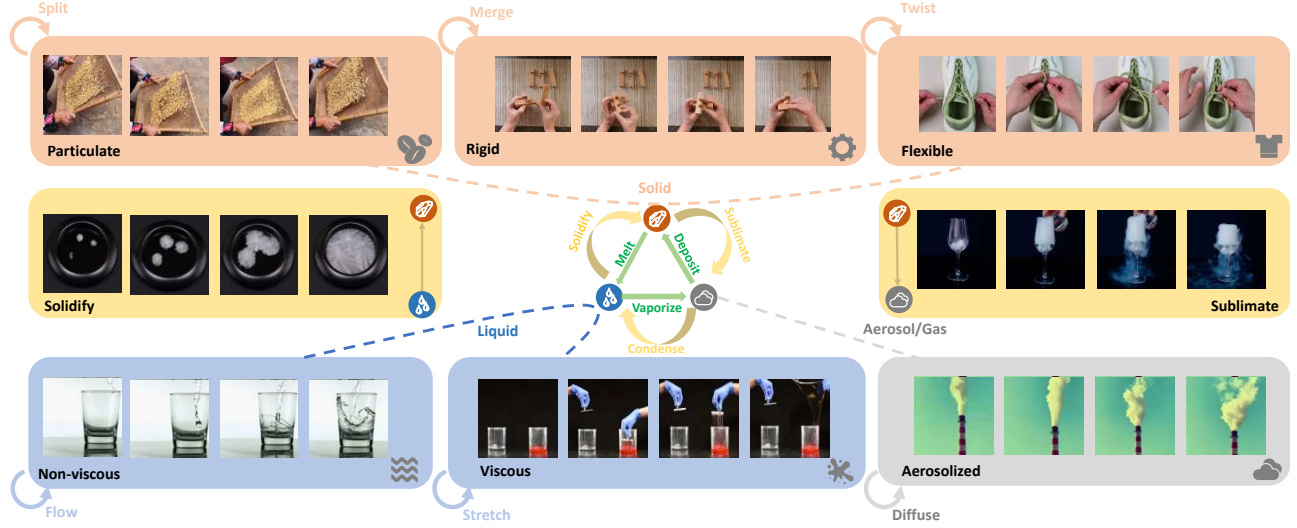


Figure 1. Objects in the real world have various phase states. Each phase has its unique transition (intra-phase transition), such as water flowing, shoelace twisting, smoke diffusing, and so on. Besides, numerous transitions occur across different phases (cross-phase transition), such as bromine liquefaction, dry ice sublimation, and water freezing.

as OCL [15] which focuses on changes in object usability, VOST [29] and VSCOS [34] which emphasize the segmentation of objects with appearance variations, most works remain limited to a single phase. They often overlook the understanding of object knowledge across phase transitions.

Thus, to address the absence of object phase transition understanding, we first categorize different objects based on their visual features and change characteristics commonly observed in daily life. Furthermore, we introduce **M³-VOS**, a fine-grained text-visual annotated dataset for object knowledge understanding across multiple scenarios, including objects that encompass a variety of transformations, including appearance changes within phases and state transitions between phases. Motivated by SA-V [25], which was constructed using the pipeline combining SAM2-assisted manual annotation with SAM2-automatic generation, we designed our semi-annotate tool based on the Interactive Demo of Cutie [4]. Besides, we propose an effective method of model cross-validation to mitigate model bias in model-assisted annotation tools.

Given the data, we analyze the current understanding of object state changes in the field of computer vision from the perspective of *Video Object Segmentation (VOS)*. On one hand, VOS task

requires the visual model to possess a comprehensive understanding of object phase knowledge to track objects that undergo significant changes in appearance and morphology during phase transitions. On the other hand, video object segmentation serves as an upstream task for other tasks, such as recognizing higher-level attributes and affordances and object manipulation tasks.

Equipped with our benchmark, we analyze state-of-the-art VOS algorithms [2, 4, 25, 33, 35]. We found significant

room for improvement in the understanding of objects undergoing phase transitions.

Additionally, by analyzing the performance differences across cases, we identified potential challenges in phase changes and proposed specific improvements, establishing a baseline **ReVOS** utilizing reverse memory, booster, and readout fusion to advance object segmentation with phase transformations.

We conclude in Sec. 6.2 by analyzing the different performances of the existing models facing different categories of phase transitions. We hope this work will motivate further exploration into more robust object knowledge understanding.

In summary, our main contributions are as follows:

1. We build a video object segmentation benchmark focused on object phase transitions, addressing the gap in understanding object phase transformations in this field.
2. We propose an efficient semi-automated annotation tool tailored for multi-phase object segmentation and a dual-model cross-validation method to address the common issue of model bias in model-assisted annotation tools.
3. To address the limitations of mainstream appearance-first models in understanding object phase transitions, we propose a bidirectional propagation module that enhances the model’s performance in this task.

2. Related Work

2.1. Object Knowledge Understanding

Recently, computer vision has seen significant advancements in object understanding, primarily represented by two paradigms. The first is the classification paradigm, which has evolved from object recognition [13] to a deeper under-

Dataset	Videos	Frames	Avg len. (s)	Ann fps.	Text	Fluid	CPT
DAVIS'16 [21]	20	1376	2.87	24	✓ [†]	✗	✗
DAVIS'17 [23]	90	6,265	2.90	24	✓ [†]	✗	✗
YTVOS [30]	982	25,812	4.38	6	✓ [†]	✗	✗
VSCOS [34]	98	44036	8.34	0.35 *	✗	✗	✗
VOST [29]	141	15,617	22.15	5	✗	✗	✗
M ³ -VOS (Ours)	479	205,181	14.27	30	✓	✓	✓

Table 1. Statistics of test set and val set in representative video segment datasets (†: DAVIS₁₆-RVOS, DAVIS₁₇-RVOS [12], Refer-YouTube-VOS [26] was built based on these datasets; *: VS-COS only annotated some frames in the valid set; Fluid: liquid or aerosol/gas phase); **CPT: Cross-Phase Transitions.** M³-VOS focuses on different phase transitions in multi-scenes, motivating our design to have a higher video annotation frame rate.

standing of object attributes [11] and affordances [10]. The second focuses on pixel-level classification, encompassing tasks such as image grounding [19, 22] and segmentation of changing objects in videos [4, 25]. The former emphasizes an explicit understanding of object knowledge, where the model is expected to extract relevant information about objects directly from images [10, 11, 13]. In contrast, the latter highlights an implicit understanding of object knowledge, where the model determines the location of objects in an image based on given prompts and its implicit recognition of object knowledge [4, 19, 22, 25].

Data-driven foundation models [17] have achieved remarkable performance in both above paradigms and even demonstrate strong open-vocabulary abilities. However, very few studies focus on understanding object phase transitions, an essential aspect of object knowledge. There is a notable lack of effective benchmarks for testing this task.

In this work, we concentrate on object phases and the corresponding **intra-phase** and **cross-phase transitions**. We construct a benchmark for the second paradigm of object knowledge understanding, designed to evaluate the capabilities of current vision models in understanding object phase transitions. This benchmark aims to fill the gap and provide a platform to test models on this critical task.

2.2. Video Object Segmentation

Video object segmentation is the process of segmenting target foreground objects from the video background at the pixel level within a video sequence. The target foreground object is typically specified either by providing a mask in the first frame, known as semi-supervised VOS [21, 23, 30].

This task requires the effective tracking of the target and a clear understanding of its boundaries, which demands that models have a thorough comprehension of the object’s appearance [21, 30], dynamic properties [29, 34], and motion information [7] within the video, as well as other physical characteristics. This is precisely why we chose video object segmentation as the specific task to evaluate the ability of vision models to understand object phase transitions.

To prompt the development of Video Object Segment, [21, 23, 30] constructs a series of early VOS benchmarks. Recently, several works have explored testing the open-world capabilities of VOS models from different perspectives: VOST [29] and VSCOS [34] focus on changes in object appearance; MeVis [7] focuses on the movement characteristics of objects. However, compared to the M³-VOS dataset, these models are all limited to single-phase objects, typically dealing with solid objects. These objects have relatively simple transformation characteristics and highly predictable movement patterns.

There are a lot of VOS methods achieve success and can be concluded into two classes:

Memory-based VOS. Semi-supervised Video Object Segmentation (SVOS) involves inference based on a ground-true mask for the first frame, and it computes the masks of the rest frames. The most frequently used methods are memory-based, which means they store pixel-level or object-level features in their memory bank and compare them with features from newly arrived frames. Recent methods [2, 3] improve the memory bank by stratifying the memory bank into short and frequently updated memories and long and infrequently updated memories to better balance efficiency and performance. Recent method Cutie [4] introduces object memory, which is fused with pixel memory in an object transformer.

Reverse propagation in VOS. We proposed a method that adopts a refinement module and optimizes the segmentation by reversely propagating the mask through the video sequence. Among the previous methods, there are not many methods that use backward mask propagation. The most similar method is DyeNet [14], which uses a re-identification module to predict a set of high-munificence masks and uses a bi-directionally proper, nation to the rest frames. Other methods that include elements of reverse optimization typically occur in bidirectional settings for sequences, e.g. bi-directional ConvLSTMs [28]. In contrast, Our method doesn’t need a high-confidence mask and is implemented as a plug-and-play module as long as the backbone is a mask propagation-based architecture.

3. Preliminary

In this section, we introduce the concept of phase and use it to classify everyday materials. Then, we categorize the transformations of objects into **Intra-Phase Transitions** and **Cross-Phase Transitions**.

3.1. Phase Categories

Rather than defining the phases of objects from the microscopic perspective provided by chemistry or physics, which focuses on molecular spacing, we adopt a *macroscopic* approach to classify objects based on their appearance and dynamic characteristics. In our study, phase refers to an

Phase			Intra-Phase Transition
Solid	Particulate		Split
	Non-Particulate	Rigid Body	Separate, Merge
Liquid	Flexible Body		Twist, Stretch
	Viscous		Stretch, Paint
Non-Viscous		Flow, Mix, Split, Paint	
Aerosol / Gas			Diffusion

Table 2. Phase definition and intra-phase transition according to visual characteristics and intrinsic transformation properties.

attribute that describes both visual characteristics and intrinsic transformation properties. Next, we categorize commonly encountered objects into three major types: *solid*, *liquid*, and *aerosol/gas*. Then we introduce the subdivided phase categories for each major class of materials, along with their respective transformation properties (Tab. 2).

For **solid materials**, particle size also influences their transformation characteristics. Therefore, we further subdivide solid materials into fragmentary or powder-like substances and non-fragmentary substances. For non-fragmentary substances, we categorize them further based on whether the material can easily undergo arbitrary deformation, dividing them into rigid and flexible objects.

For **liquid materials**, substances like melted cheese or melted rubber do not frequently exhibit fluidity in everyday situations. Instead, they demonstrate viscous properties, such as stringiness, when interacting with other materials. Therefore, we classify liquid materials based on their degree of fluidity and viscosity, dividing them into viscous and non-viscous substances.

For **aerosols/gases**, it not only includes common gaseous substances but also solid particles and liquid droplets suspended in the air. These materials possess the property of continuous diffusion in the atmosphere.

3.2. Phase Transition

In everyday life, objects undergo various changes through interactions with the environment or humans. Based on whether these changes cross different phase states, we categorize them into *intra-phase* and *cross-phase* transitions.

Intra-Phase Transformations primarily depend on the transformation characteristics inherent to the phase state of the object itself. Different phase states of materials often exhibit unique intra-phase transformations. For example, flexible solids can be twisted (*e.g.*, shoelaces or knots), viscous substances can stretch (*e.g.*, melted cheese or syrup), and aerosols/gases can diffuse (smoke or steam diffusion).

Cross-Phase Transformations are quite common in everyday life but are often overlooked. Due to the differences in phase states before and after the transformation, these objects exhibit distinctly different visual characteristics and transformation properties. Therefore, understanding such transformations poses a greater challenge.

In Supplementary, we provide more detailed definitions of these phases and phase transition.

4. Dataset Design and Construction

In this section, we introduce the data collection and annotation of M³-VOS. The key steps include selecting representative videos, annotating them with instance masks and information text, and defining an evaluation protocol.

4.1. Video Collection

We chose to source our videos from YouTube and BiliBili mainly, where there are lots of videos about intra-phase transition and cross-phase transition in different scenery: kitchen, outdoor, factory, school, farm, *etc*. In total, **14 scenarios** as shown in Fig. 2a. In these scenarios, target objects undergo intra-phase transitions or cross-phase transitions as they engage in various interactions, including interactions with humans, other objects, and the environment.

Most of the internet videos were captured using consumer cameras. To better capture rapid and dramatic phase transitions, such as balloon bursts or glass shattering, we also collected **high-frame-rate** video clips shot with high-speed cameras. For slower phase transitions, like ice melting or frost formation, we gathered a portion of **low-frame-rate** video clips taken with time-lapse techniques.

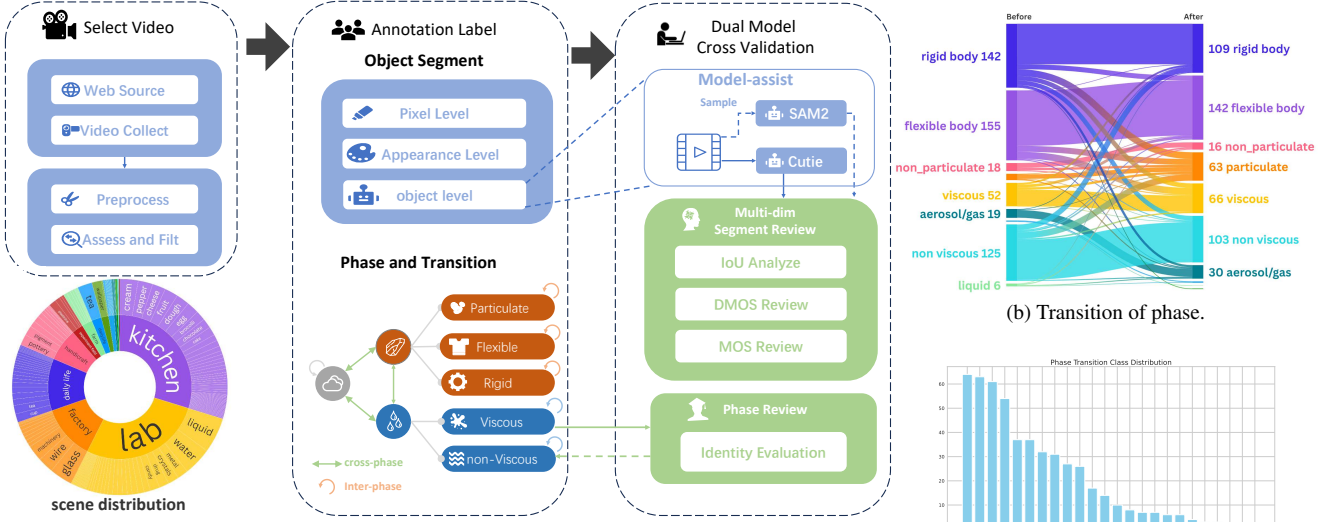
Next, we performed temporal cutting and spatial cropping to focus more on the process of phase transitions. The videos have an average length of 14.27 seconds. To further enrich the scenarios in our dataset, we collected a portion of videos filmed in the laboratory. We have carefully checked all the videos to avoid possible ethnic problems and will only provide access through video URLs along with downloadable preprocessing scripts.

4.2. Annotation Design

Each video clip is accompanied by rich annotations for target segmented objects, identifying the corresponding phase transitions. This includes a bilingual (Chinese and English) description of one or more target objects in each clip, the phases of each target object in the first and last frames, as well as pixel-level segmentation annotations with 30 fps.

In video collection, we instructed the video collectors to use clear and accurate positional terms to describe each target object in the first frame. The descriptions are “*In the process of [specific action], the [specific object] which at [specific location] in the initial frame or whose color is [specific color].*” , providing accurate guidance for the volunteers responsible for the mask annotations.

In the annotation, we instructed volunteers to use the information provided by the video collectors about the target objects and the semi-auto Annotation Tool (detailed in Sec. 4.3.1) to annotate the masks of the target objects in



(a) Dataset construction. The core pipeline component is a multi-level semi-auto segmentation tool including Eraser Brush (**pixel-level**), Color Difference Mask (**appearance-level**), and Model-Assisted Annotation (**object-level**), enabling the efficient annotation of objects with complex phase transitions.

Figure 2. M³-VOS characteristics. (a) M³-VOS dataset pipeline including annotating and dual model cross-valid method for model-bias. (b) Transition from before phase (left) to after phase (right). (c) Distribution of the phase transition in the M³-VOS.

each frame of the video. For various *uncertain* void masks caused by unclear image quality or motion blur,

we instructed volunteers to annotate the corresponding void masks, similar to the approach in the VOST [29]. In this way, we can disregard the influence of these pixels during the evaluation process. Volunteers were also required to select the *initial* and *final* phases of the target objects from Tab. 2 based on their states in the video, and subsequently label the corresponding phase transformations.

4.3. Annotation Collection

In this section, we introduce our semi-auto Annotation tool which efficiently annotates the masks of target objects in the videos, and our annotation collection pipeline.

4.3.1. Semi-Auto Multi-Level Annotation Tool

To efficiently annotate the masks of target objects in the videos, we employed a semi-automated multi-level annotation tool that utilizes a paint-erase tool (**pixel-level**), pixel color difference assistance (**appearance-level**), and neural network-based annotation support (**object-level**).

Our annotation tool mainly employs a *paint-and-erase* approach. Volunteers can use a brush and eraser tool, along with a magnification feature, to accurately annotate the masks of target objects and the void masks in the video. To achieve high-frame-rate mask annotation, we integrated the fully automated annotation tool provided by Cutie [4] based on RITM [27] for interactive image segmentation and Cutie for video object segmentation. After volunteers annotate masks for a specific frame using the paint-and-erase approach or point prompt method, they can utilize Cutie to

propagate masks for that frame. Subsequently, the propagated pseudo-ground truth can be refined using the paint-and-erase approach. The *neural network based* automatic annotation tool provides good pseudo ground truth references for objects with clear contours. However, the tool often fails to provide satisfactory pseudo-ground truth for target objects like water vapor, thick smoke, and splashes, which have unclear outlines. Thus, our tool integrates a *color difference masking*, allowing users to select a specific pixel value in the image and set a range to create a color difference template for the video.

Given a pixel p_s and any other pixel p_i , the position of p_i will be labeled according to

$$M(p_i) = \begin{cases} 1 & \iff \begin{aligned} \Delta H_s(p_i) &< 0.1\delta, \\ \Delta S_s(p_i) &< \delta, \\ \Delta V_s(p_i) &< \delta, \end{aligned} \\ 0 & \text{otherwise.} \end{cases} \quad (1)$$

$$\Delta \phi_s(p_i) = |\phi(p_i) - \phi(p_s)|, \quad \phi \in \{H, S, V\}.$$

We label the pixel p_i if and only if the color difference between p_s and p_i is within 0.1δ , and the differences in saturation and brightness are within δ . Here, δ is a user-adjustable parameter.

Our testing has shown that this functionality effectively annotates objects with unclear contours but distinct colors, especially for gases and liquids.

4.3.2. Annotation Pipeline and Statistics

As illustrated in Fig. 2a, in our annotation pipeline, we hired 12 volunteers and provided them with 7 days of training to use the annotation tools on the videos we collected.

To ensure the quality of the data annotations, we employed 3 experienced reviewers to audit the annotated data. Each volunteer’s masks were evaluated based on three criteria: tracking accuracy, completeness of annotation, and boundary stability, scored on a scale from 0 to 3 (detailed scoring criteria and the review result can be found in the Supplement). The final mask review score was the average of the two reviewers’ ratings. If any score is below 2, we consider the mask Unqualified. In addition to the MOS reviewing, we employed a dual-model cross-validation approach to verify the annotated masks (detailed in Sec. 4.4). If the validated mask annotations do not meet the quality standards, we require the volunteer to annotate again until the review is approved.

Overall, we collect **205,181** masks, with an average track duration of **14.27s**. M³-VOS covers **120+** categories of objects across **6** phases within a total of **14** scenarios, encompassing **23** specific phase transitions. We report additional statistics in Figs. 2b and 2c.

4.4. Avoidance of Model Bias

Although using Cutie to generate pseudo-ground truth significantly improves the annotation efficiency, it’s crucial to thoroughly verify whether the volunteers’ refinements of the pseudo-ground truth can effectively mitigate the model bias introduced by Cutie. Therefore, we introduce our method for ensuring that the annotated masks are free from bias via dual model cross-validation.

In this process, we sample around 20% video clips in M³-VOS and require half of our volunteers to annotate the masks using another self-implement SAM2-assist tool. Meanwhile, they are required to label masks secondly using the Cutie-assist tool. Finally, we compare three kinds of masks from the two subjective qualitative and the objective quantitative aspects. In this way, we demonstrate that our dataset pipeline effectively mitigates the model bias and that the model bias of mask annotations in M³-VOS is negligible. The details of the process and result can be found.

4.5. Core Subset

To facilitate analysis of the challenge facing the phase transition in the VOS task, we extracted video clips that humans consider to be highly representative and comprehensive in variety. Finally, we split M³-VOS into two subsets for evaluation, including the full subset and core subset. The details can be found in Supplementary.

5. Method

In data collection and annotation, we observed that when objects undergo intra-phase or cross-phase transitions, their inherent *disorder* tends to increase. This hidden phenomenon makes mask predictions increasingly more difficult. If the final state of the object at the end of the video is

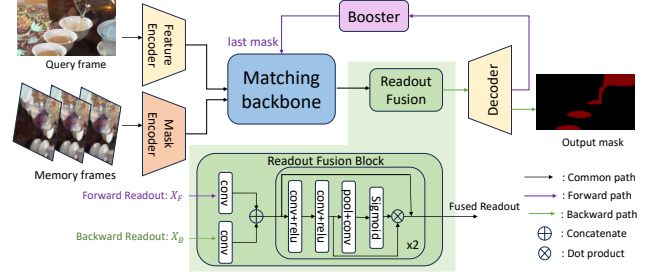


Figure 3. Overview of our ReVOS. ReVOS is a *plug-and-play* based on propagation-based matching backbones. ReVOS includes a Booster Module and a Readout Fusion Module. The forward and reverse pathway is shown in purple and green separately.

well annotated, *reverse-propagating* to predict the mask becomes more accurate. We hypothesize that this is because the reverse process involves a gradual reduction in disorder, which simplifies segmentation.

Given an object in a specific frame, We use Local Binary Pattern (LBP) [20] of its mask to describe its entropy. By isolating the object from the background, we create a binary image G . If we calculate the LBP values of all pixels in G , we obtain a histogram H , where $H(i)$ represents the frequency of the LBP value i . then h_{LBP} can be formulated as Eq. (2):

$$h_{LBP} = - \sum_{i=0}^{N-1} H(i) \log_2 H(i). \quad (2)$$

We calculated the average h_{LBP} for the masks in the first and second halves of several datasets. The results are shown in Tab. 3. In most datasets, the h_{LBP} values in the latter half are higher than those in the first half, which supports our hypothesis.

Given this, we propose a paradigm to improve performance using reverse-propagation. We introduce a *plug-and-play* framework named ReVOS based on mask propagation backbones (Fig. 3). We consider only the single target object as the multi-object scenarios are easily derived. First, the model performs a forward propagating pipeline based on the matching backbone, where the last output mask will be boosted and re-introduced into the model. Then the model will perform **reverse propagation** on a sliding window of previous frames. The object readout of the forward and reverse pipeline will be *fused* in the Readout Fusion Module to generate better results. In the following, we describe the three main contributions of ReVOS.

Reverse Memory. In the forward propagation of the mask, we maintain a sliding window of length T . Suppose the model needs to predict the t -th frame as the current time. The sliding window includes image information from $\max(0, t - T)$ to $\max(0, t - 1)$ and the extracted forward memory readout. The reverse memory is similar to working

Dataset	M ³ -VOS	VOST	YouTube VOS-2019 val	DAVIS' 17 val
First half	4.28	4.29	4.32	4.72
Latter half	4.37	4.48	4.35	4.68

Table 3. h_{LBP} of the first half and the latter half of VOS datasets.

memory in [2]. The difference is that it only stores high-resolution features for the reverse process, serving the same function as working memory in the reverse propagation. It is cleared at the beginning of each reverse propagation as we want the reverse memory to only collect information from the current reverse process.

Booster. if the model loses information about the mask for certain object parts during the forward process, this loss will be taken into the reverse process and continue to adversely affect the segmentation results. To address this issue, we implement a strategy to boost the mask during forward propagation. This enhancement aims to predict as many locations as possible, thereby reducing local mask loss. The boosted mask will be re-input into the matching backbone to generate the next frame mask. In the implementation, we output the final mask via

$$M = \sigma(\alpha X_{decode}), \quad (3)$$

where α is boosting factor, σ is sigmoid function, X_{decode} is the decoded logits, M is the boosted mask.

Readout Fusion. In the forward and reverse process, readout features will be extracted from the matching backbone. To obtain the final mask, we design a Fusion module to integrate readout features from the forward process, as shown in Fig. 3.

5.1. Implementation Details

We adopt Cutie-base [4] as our matching backbone, which is trained under “MEGA” setting with 5 datasets: YoutubeVOS [31], DAVIS [21], BURST [1], OVIS [24], and MOSE [8]. In training, we froze all the parameters of Cutie and only trained the Readout Fusion Module. We finetune our model with AdamW [18] optimizer. The learning rate is set to 1e-5. Finetuning takes about 75k iterations and we reduce the learning rate by 10 times after 60K and 67.5K iterations. The model is trained on 4 A100 GPUs for 10 hours.

6. Analysis

In evaluation, we adopt standard metric Jaccard index \mathcal{J} , newly proposed metrics \mathcal{J}_{tr} [29] and \mathcal{J}_{cc} [34]. \mathcal{J}_{tr} represents the Jaccard index of the last 25% frames and \mathcal{J}_{cc} represents the Jaccard index based on each connected component and takes an average over all components. For YouTubeVOS [31], we use its official metrics: \mathcal{J} and \mathcal{F} for seen and unseen categories. \mathcal{G} is the averaged \mathcal{J} & \mathcal{F} for both seen and unseen classes.

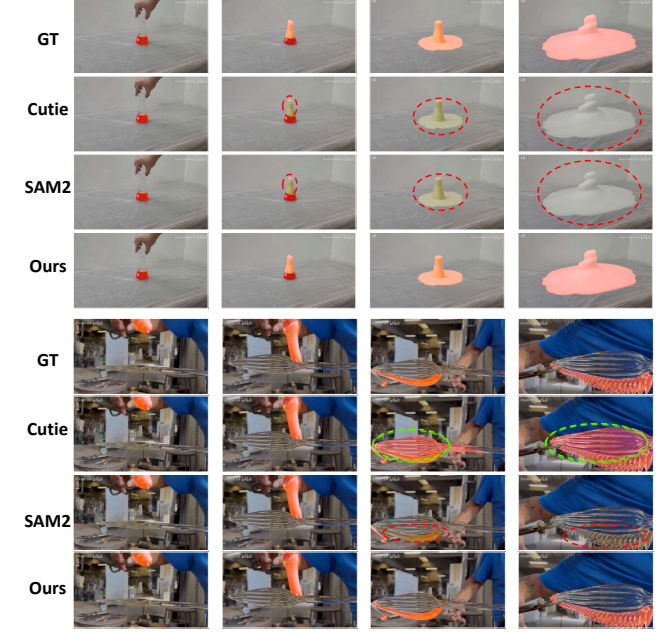


Figure 4. Visualization of qualitative results. (Red circle: false-negative region; Green circle: false-positive region). The highlight color region is the predicted mask. Phase transitions, e.g., reagent eruptions and glass solidification, challenge current models in boundary prediction, causing tracking failures or background interference. However, Our reverse inference correction effectively addresses these issues.

6.1. Main Results

We compare ReVOS with SOTA approaches on our dataset and standard benchmarks: VOST validation [29] DAVIS 2017 validation [23] and YouTubeVOS validation [30]. For our dataset, we create two versions: M³-VOS full (all cases) and M³-VOS core (highly representative cases). For a fair comparison and open-vocabulary purpose, we choose only one checkpoint that each method performs the best on the DAVIS 2017 validation set and use it to test all other datasets. For DeAOT, we excluded a few long video cases as we encountered insufficient memory during inference.

In Tab. 4, ReVOS achieves better results than all SOTA methods, especially on our dataset. As we freeze the Cutie backbones during training, it is evident that the increase in our model’s score relative to Cutie is entirely due to our new framework. Specifically, SAM2 achieved the best result on VOST. We assume it takes more training data similar to EPIC-kitchens [5] from which the VOST is constructed.

6.2. Intra-Phase vs. Cross-Phase Transformations

We present the average model performance in 4 categories: Intra-Phase (solid), Intra-Phase (Liquid), Intra-Phase (Aerosol/Gas), and Cross-Phase, which are abbreviated as IS, IL, IG and CP in Tab. 5. In addition, we also

	M ³ -VOS full			M ³ -VOS core			VOST val			DAVIS'17 val			YouTubeVOS-2019 val				
	\mathcal{J}	\mathcal{J}_{tr}	\mathcal{J}_{cc}	\mathcal{J}	\mathcal{J}_{tr}	\mathcal{J}_{cc}	\mathcal{J}	\mathcal{J}_{tr}	\mathcal{J}_{cc}	\mathcal{J}	\mathcal{J}_{tr}	\mathcal{J}_{cc}	\mathcal{G}	\mathcal{J}_s	\mathcal{F}_s	\mathcal{J}_u	\mathcal{F}_u
DeAOT * [33]	72.5	65.2	61.2	62.3	55.1	51.4	45.6	33.2	35.1	82.7	79.8	60.9	86.2	85.6	90.6	80.0	88.4
XMem [2]	70.4	61.5	58.8	60.6	50.6	49.2	36.0	24.8	26.6	82.9	81.3	61.3	85.4	84.3	88.6	80.3	88.5
RMem + DeAOT [†] [35]	73.4	66.1	62.6	56.1	45.5	46.7	40.5	25.3	31.9	82.3	79.3	60.9	85.9	84.6	89.4	80.8	88.9
SAM2 [25]	69.5	57.8	58.2	61.0	49.9	48.9	44.1	28.0	32.7	85.5	82.8	64.1	85.2	83.7	80.6	87.9	88.5
Cutie-base [4]	74.6	64.6	64.3	64.6	52.0	53.9	40.8	25.1	31.6	85.6	84.6	63.9	86.8	85.9	90.4	81.6	89.3
Ours	75.6	66.5	65.2	66.3	55.8	55.5	41.0	25.3	31.7	86.0	84.8	64.2	86.8	85.3	89.8	82.1	89.9

Table 4. Comparison of semi-VOS methods. The metrics are \mathcal{J} , \mathcal{J}_{tr} , and \mathcal{J}_{cc} for M³-VOS (full, core), VOST, and DAVIS'17 ([†]: R50-DeAOT-L with restricted memory bank without temporal position embedding; *: SwinB-DeAOT-L; the grep region contains 469 objects. The Video clip of Other Objects is too long. DeAOT doesn't support long videos due to the memory limitation).

	IS			IL			IG			CP		
	\mathcal{J}	\mathcal{J}_{tr}	\mathcal{J}_{cc}									
DeAOT [33]	71.6	64.7	59.8	72.1	65.0	59.9	80.0	74.3	67.9	73.8	66.0	65.3
XMem [2]	70.9	62.8	58.9	68.2	58.7	56.1	80.2	71.3	64.7	74.5	66.4	65.4
Rmem + DeAOT [35]	74.5	67.3	63.3	71.3	63.6	59.8	83.5	82.0	68.5	77.0	70.4	68.3
SAM2 [25]	64.7	52.6	54.7	69.8	57.7	57.6	67.6	57.4	56.1	74.2	63.9	64.0
Cutie-base [4]	72.3	61.7	62.5	74.1	64.1	63.3	75.8	64.3	63.6	77.5	69.7	69.0
Ours	73.0	63.2	63.3	75.6	66.4	64.2	76.8	66.5	65.4	78.1	70.8	69.6

Table 5. Performance of different VOS methods in phase transitions.

present the performance of our model for the detailed phase transitions in Fig. 5.

Compared to pure Cutie, Our Cutie-ReVOS improves the performance in all phase transitions. Compared to the SOTA, Cutie-ReVOS still demonstrated excellent performance facing these phase transitions. Especially, when facing the cross-phase transition, Cutie-ReVOS achieves the best performance in all models we have evaluated.

6.3. Performance Differences across Benchmarks

Compared to existing benchmarks, M³-VOS significantly expands the phase range of objects, introducing a series of new challenges for tracking and segmentation. For example, M³-VOS includes liquids and granular solids, where target objects often exhibit rapid motion due to splashing or splitting. A large portion of fluids (both gases and liquids) also tend to be transparent, and phase transitions are often accompanied by changes in the object's appearance and color. As Tab. 4 demonstrate, the performance of all existing models showed a significant decline.

Especially, comparing the full M³-VOS full set and the M³-VOS core subset, which balances the distribution of scene and phase transition, the existing modes have more obvious performance deficiencies. This phenomenon shows that the current models all have a certain degree of scenery bias and phase bias.

6.4. Ablation Study

We study various designs of our algorithm in the ablation. We report \mathcal{J} , \mathcal{J}_{tr} and \mathcal{J}_{cc} and FPS for M³-VOS mid set.

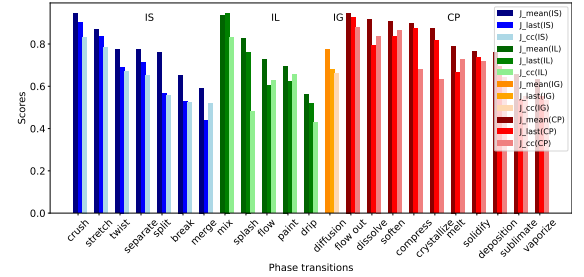


Figure 5. Results of ReVOS on phase transitions.

Setting	\mathcal{J}	\mathcal{J}_{tr}	\mathcal{J}_{cc}	FPS
<i>Sliding window length</i>				
10	75.6	66.6	65.2	15.3
30	75.7	66.4	65.3	15.4
60	75.4	66.3	65.0	10.4
<i>Reverse interval</i>				
10	75.5	66.5	65.1	7.9
30	75.7	66.4	65.3	15.4
60	75.7	66.7	65.4	21.6

Table 6. Comparison with different hyperparameters.

Setting	\mathcal{J}	\mathcal{J}_{tr}	\mathcal{J}_{cc}
Only forward (Cutie)	74.7	64.6	64.5
Only backward	75.4	66.4	64.9
With readout fusion	75.7	66.4	65.3
Without booster	74.2	64.2	63.9
With booster	75.7	66.4	65.3

Table 7. Ablation on Booster and Readout Fusion Module.

Hyperparameter Choices. Tab. 6 compares our results with different choices of hyperparameters: sliding window length T and reverse interval L . Note that $T = 0$ or $L = 0$ is equivalent to Cutie-base. T is fixed to 30 when we vary the value of L and vice versa. We find that a larger sliding window length means high performance but also implies a decrease in FPS. Surprisingly, a larger reverse interval also means higher performance with an increase in FPS. Tab. 7 shows that the performance improvement brought by the booster and readout fusion demonstrates the necessity of adding these modules.

7. Discussion and Limitations

Annotation Bias. Annotation bias is inevitably introduced by annotators' tendencies, inherent biases in assisted tools, and ambiguous regions in videos. As discussed in Sec. 4.4, despite our implementation of multi-round, multi-level review processes, some discrepancies remain across annotation instances. Establishing a more standardized and rigorous data annotation review workflow could effectively mitigate annotation bias.

Model Performance. All models show limitations on our new benchmark with challenging object phase transitions. In future works, models may be advanced by leveraging the physical knowledge embedded in MLLMs.

8. Conclusion

In this work, we explored the ability of the visual models to understand object phase transitions through a video segmentation task, introducing a fine-grained text-visual annotated open-vocabulary benchmark M³-VOS. It includes 14 scenes, encompassing 120+ objects across 6 phase states and 23 phase transitions (13 intra-phases, 10 inter-phases). To address the limitations of existing methods, we proposed a plug-and-play module ReVOS based on entropy theory, achieving decent improvements in M³-VOS and comparable performance on other benchmarks. However, effectively understanding phase transitions remains a challenge. We believe this will pave the way for a new direction in research focused on a deeper understanding of objects.

References

- [1] Ali Athar, Jonathon Luiten, Paul Voigtlaender, Tarasha Khurana, Achal Dave, Bastian Leibe, and Deva Ramanan. Burst: A benchmark for unifying object recognition, segmentation and tracking in video. In *Proceedings of the IEEE/CVF winter conference on applications of computer vision*, pages 1674–1683, 2023. 7
- [2] Ho Kei Cheng and Alexander G Schwing. Xmem: Long-term video object segmentation with an atkinson-shiffrin memory model. In *European Conference on Computer Vision*, pages 640–658. Springer, 2022. 2, 3, 7, 8
- [3] Ho Kei Cheng, Yu-Wing Tai, and Chi-Keung Tang. Rethinking space-time networks with improved memory coverage for efficient video object segmentation. *Advances in Neural Information Processing Systems*, 34:11781–11794, 2021. 3
- [4] Ho Kei Cheng, Seoung Wug Oh, Brian Price, Joon-Young Lee, and Alexander Schwing. Putting the object back into video object segmentation. In *Proceedings of the IEEE/CVF Conference on Computer Vision and Pattern Recognition*, pages 3151–3161, 2024. 2, 3, 5, 7, 8
- [5] Dima Damen, Hazel Doughty, Giovanni Maria Farinella, Sanja Fidler, Antonino Furnari, Evangelos Kazakos, Davide Moltisanti, Jonathan Munro, Toby Perrett, Will Price, et al. Scaling egocentric vision: The epic-kitchens dataset. In *Proceedings of the European conference on computer vision (ECCV)*, pages 720–736, 2018. 7
- [6] Jia Deng, Wei Dong, Richard Socher, Li-Jia Li, Kai Li, and Li Fei-Fei. Imagenet: A large-scale hierarchical image database. In *2009 IEEE conference on computer vision and pattern recognition*, pages 248–255. Ieee, 2009. 1
- [7] Henghui Ding, Chang Liu, Shuting He, Xudong Jiang, and Chen Change Loy. Mevis: A large-scale benchmark for video segmentation with motion expressions. In *Proceedings of the IEEE/CVF International Conference on Computer Vision*, pages 2694–2703, 2023. 3
- [8] Henghui Ding, Chang Liu, Shuting He, Xudong Jiang, Philip HS Torr, and Song Bai. Mose: A new dataset for video object segmentation in complex scenes. In *Proceedings of the IEEE/CVF International Conference on Computer Vision*, pages 20224–20234, 2023. 7
- [9] Hao-Shu Fang, Jianhua Sun, Runzhong Wang, Minghao Gou, Yong-Lu Li, and Cewu Lu. Instaboost: Boosting instance segmentation via probability map guided copy-pasting. In *ICCV*, 2019. 2
- [10] James J Gibson. The ecological approach to the visual perception of pictures. *Leonardo*, 11(3):227–235, 1978. 1, 3
- [11] Phillip Isola, Joseph J Lim, and Edward H Adelson. Discovering states and transformations in image collections. In *Proceedings of the IEEE conference on computer vision and pattern recognition*, pages 1383–1391, 2015. 1, 3
- [12] Anna Khoreva, Anna Rohrbach, and Bernt Schiele. Video object segmentation with language referring expressions. In *Computer Vision–ACCV 2018: 14th Asian Conference on Computer Vision, Perth, Australia, December 2–6, 2018, Revised Selected Papers, Part IV 14*, pages 123–141. Springer, 2019. 3
- [13] Alex Krizhevsky, Ilya Sutskever, and Geoffrey E Hinton. Imagenet classification with deep convolutional neural networks. *Advances in neural information processing systems*, 25, 2012. 1, 2, 3
- [14] Xiaoxiao Li and Chen Change Loy. Video object segmentation with joint re-identification and attention-aware mask propagation. In *Proceedings of the European conference on computer vision (ECCV)*, pages 90–105, 2018. 3
- [15] Yong-Lu Li, Yue Xu, Xinyu Xu, Xiaohan Mao, Yuan Yao, Siqi Liu, and Cewu Lu. Beyond object recognition: A new benchmark towards object concept learning. In *Proceedings of the IEEE/CVF International Conference on Computer Vision*, pages 20029–20040, 2023. 2
- [16] Tsung-Yi Lin, Michael Maire, Serge Belongie, James Hays, Pietro Perona, Deva Ramanan, Piotr Dollár, and C Lawrence Zitnick. Microsoft coco: Common objects in context. In *Computer Vision–ECCV 2014: 13th European Conference, Zurich, Switzerland, September 6–12, 2014, Proceedings, Part V 13*, pages 740–755. Springer, 2014. 1
- [17] Haotian Liu, Chunyuan Li, Yuheng Li, and Yong Jae Lee. Improved baselines with visual instruction tuning, 2024. 3
- [18] I Loshchilov. Decoupled weight decay regularization. *arXiv preprint arXiv:1711.05101*, 2017. 7
- [19] Junhua Mao, Jonathan Huang, Alexander Toshev, Oana Camburu, Alan Yuille, and Kevin Murphy. Generation and comprehension of unambiguous object descriptions, 2016. 3
- [20] Timo Ojala, Matti Pietikäinen, and Topi Mäenpää. Multiresolution gray-scale and rotation invariant texture classification with local binary patterns. *IEEE Transactions on Pattern Analysis and Machine Intelligence*, 24(7):971–987, 2002. 6
- [21] Federico Perazzi, Jordi Pont-Tuset, Brian McWilliams, Luc Van Gool, Markus Gross, and Alexander Sorkine-Hornung. A benchmark dataset and evaluation methodology for video object segmentation. In *Proceedings of the IEEE conference on computer vision and pattern recognition*, pages 724–732, 2016. 3, 7

[22] Bryan A. Plummer, Liwei Wang, Chris M. Cervantes, Juan C. Caicedo, Julia Hockenmaier, and Svetlana Lazebnik. Flickr30k entities: Collecting region-to-phrase correspondences for richer image-to-sentence models, 2016. 3

[23] Jordi Pont-Tuset, Federico Perazzi, Sergi Caelles, Pablo Arbelaez, Alexander Sorkine-Hornung, and Luc Van Gool. The 2017 davis challenge on video object segmentation. *arXiv:1704.00675*, 2017. 3, 7

[24] Jiyang Qi, Yan Gao, Yao Hu, Xinggang Wang, Xiaoyu Liu, Xiang Bai, Serge Belongie, Alan Yuille, Philip HS Torr, and Song Bai. Occluded video instance segmentation: A benchmark. *International Journal of Computer Vision*, 130(8):2022–2039, 2022. 7

[25] Nikhila Ravi, Valentin Gabeur, Yuan-Ting Hu, Ronghang Hu, Chaitanya Ryali, Tengyu Ma, Haitham Khedr, Roman Rädle, Chloe Rolland, Laura Gustafson, et al. Sam 2: Segment anything in images and videos. *arXiv preprint arXiv:2408.00714*, 2024. 2, 3, 8

[26] Seonguk Seo, Joon-Young Lee, and Bohyung Han. Urvos: Unified referring video object segmentation network with a large-scale benchmark. In *Computer Vision–ECCV 2020: 16th European Conference, Glasgow, UK, August 23–28, 2020, Proceedings, Part XV 16*, pages 208–223. Springer, 2020. 3

[27] Konstantin Sofiiuk, Ilia A. Petrov, and Anton Konushin. Reviving iterative training with mask guidance for interactive segmentation, 2021. 5

[28] Hongmei Song, Wenguan Wang, Sanyuan Zhao, Jianbing Shen, and Kin-Man Lam. Pyramid dilated deeper convlstm for video salient object detection. In *Proceedings of the European conference on computer vision (ECCV)*, pages 715–731, 2018. 3

[29] Pavel Tokmakov, Jie Li, and Adrien Gaidon. Breaking the “object” in video object segmentation. In *Proceedings of the IEEE/CVF Conference on Computer Vision and Pattern Recognition*, pages 22836–22845, 2023. 2, 3, 5, 7

[30] Ning Xu, Linjie Yang, Yuchen Fan, Jianchao Yang, Dingcheng Yue, Yuchen Liang, Brian Price, Scott Cohen, and Thomas Huang. Youtube-vos: Sequence-to-sequence video object segmentation, 2018. 3, 7

[31] Ning Xu, Linjie Yang, Yuchen Fan, Dingcheng Yue, Yuchen Liang, Jianchao Yang, and Thomas Huang. Youtube-vos: A large-scale video object segmentation benchmark. *arXiv preprint arXiv:1809.03327*, 2018. 7

[32] Wenqiang Xu, Yonglu Li, and Cewu Lu. Srda: Generating instance segmentation annotation via scanning, reasoning and domain adaptation. In *ECCV*, 2018. 2

[33] Zongxin Yang and Yi Yang. Decoupling features in hierarchical propagation for video object segmentation. *Advances in Neural Information Processing Systems*, 35:36324–36336, 2022. 2, 8

[34] Jiangwei Yu, Xiang Li, Xinran Zhao, Hongming Zhang, and Yu-Xiong Wang. Video state-changing object segmentation. In *Proceedings of the IEEE/CVF International Conference on Computer Vision*, pages 20439–20448, 2023. 2, 3, 7, 1

[35] Junbao Zhou, Ziqi Pang, and Yu-Xiong Wang. Rmem: Restricted memory banks improve video object segmentation. In *Proceedings of the IEEE/CVF Conference on Computer Vision and Pattern Recognition*, pages 18602–18611, 2024. 2, 8

M^3 -VOS: Multi-Phase, Multi-Transition, and Multi-Scenery Video Object Segmentation

Supplementary Material

Overview

We introduce:

- More implementation details of our work in Secs. 9 to 14.
- More experiments about the challenge in M^3 -VOS in Sec. 15.
- More failure cases in Sec. 16.

9. Details of Annotations

9.1. Phase Definition

We list the specific definitions of phase below:

- **Solid:** Volume is relatively fixed, has distinct boundaries, and shapes independent of the container.
 - **Particulate:** Composed of several fragmented parts.
 - **Non-particulate:** Composed of single/few larger parts.
 - * **Rigid Body:** Exhibiting a relatively fixed shape and resistance to deformation.
 - * **Flexible Body:** Has a relatively unstable shape and can undergo deformation easily.
- **Liquid:** Volume is relatively fixed and has distinct boundaries, fluidity, or shape dependent on the container.
 - **Viscous Fluid:** Has significant viscosity, and can stretch.
 - **Non-viscous Liquid:** No significant viscosity, cannot stretch.
- **Aerosol/Gas:** Volume not fixed, has no distinct boundaries, shape dependent on the container.

9.2. Phase Transition Definition

In our works, we ensure that the definition of phase transitions meets a fundamental requirement: the transition from an initial state to a final state may correspond to different specific phase transitions depending on the characteristics of the transformation. However, for a specific phase transition, its initial and final states must be unique.

We list all the initial and final states for each phase transition as Tab. 8. Besides, in Tab. 9, we give a detailed definition of different phase transitions.

10. Connected Component Jaccard Index

To avoid ignorance of the small part during evaluation, we introduce the connect component Jaccard Index \mathcal{J}_{cc} . The definition of \mathcal{J}_{cc} is the average Jaccard Index of the maximum bipartite matching corresponding to all connected

mask components between the ground truth and the predicted image.

We implemented our \mathcal{J}_{cc} using the *Hungarian* algorithm, different from the one in the official implementation of VSCOS [34] that calculates the \mathcal{J}_{cc} using a two-loop matching process, *i.e.*, iteratively finding for each connected component in Mask A the one in Mask B that maximizes the Jaccard Index.

11. Details of Masks SQA

11.1. Three Criteria in Masks SQA

We design three criteria to evaluate the annotation in M^3 -VOS, including:

- **Tracking Accuracy**
 - 0: Target is lost or tracked incorrectly for a long time.
 - 1: Target is lost or tracked incorrectly for a short continuous period.
 - 2: Target is lost or tracked incorrectly in a few isolated frames.
 - 3: **Target is always tracked correctly.**
- **Mask Annotation Completeness**
 - 0: Mask has been completely missing for a long time.
 - 1: Mask has been partially missing for a long time.
 - 2: Mask is partially missing in some frames.
 - 3: **Mask is complete and accurate throughout.**
- **Mask Boundary Stability**
 - 0: Mask boundary shows an obvious jitter for a long time.
 - 1: Mask boundary shows a slight jitter for a long time.
 - 2: Mask boundary shows a slight jitter for a short time.
 - 3: **Mask boundary shows no visible jitter.**

11.2. SQA Analyze

We select three experienced reviewers to evaluate all of our masks in M^3 -VOS in the criteria of Sec. 11.1 using the reviewer UI as Fig. 6. In the process of constructing M^3 -VOS, we make sure the scores in any criterion of all of our masks are higher than 2. In the final evaluation of M^3 -VOS, the MOS in these criteria are 2.95 in tracking accuracy, 2.91 in mask annotation completeness, and 2.89 in mask boundary stability.

12. Details of Avoidance of Model Bias

In this part, we introduce the details of the dual-model cross-validation method. In this process, we validate that

Table 8. The different phase transitions and the unique initial state and final state. We give some examples to highlight their characteristic.

Category	Phase Transition	Initial State	Final State	Example
Intra-Phase (Solid)	Separate	Rigid	Rigid	<i>Disassembling a gun, Taking apart building blocks</i>
	Twist	Flexible	Flexible	<i>Knead dough, Tie shoelaces</i>
	Break	Rigid	Particulate	<i>Break cups, Chop vegetables</i>
	Stretch	Flexible	Flexible	<i>Pull noodles, Pull rubber</i>
	Split	Particulate	Particulate	<i>Sift the rice, Sieve the sand</i>
	Merge	Rigid	Rigid	<i>assemble guns, Jigsaw puzzle</i>
Intra-Phase (Liquid)	Crush	Rigid	Particulate	<i>Grind the herb, Crush the stone</i>
	Flow	Non-Viscous	Non-Viscous	<i>Pour Water, Pour tea</i>
	Paint	Liquid	Liquid	<i>Paint the wall, Paint in oil</i>
	Splash	Non-Viscous	Non-Viscous	<i>Diving sports, Cast a stone into the water</i>
	Mix	Non-Viscous	Non-Viscous	<i>Milk pouring art, Paint mixing with water</i>
Intra-Phase (Aerosol/Gas)	Drip	Non-Viscous	Non-Viscous	<i>Drip the acid, Drip the eye drops</i>
	Diffuse	Aerosol/Gas	Aerosol/Gas	<i>Smoke spreads, Mist spreads</i>
Cross-Phase	Solidify	Liquid	Solid	<i>Water freezes, Chocolate hardens into solid chocolate</i>
	Melt	Solid	Liquid	<i>Melt chocolate, Melt the ice</i>
	Deposition	Aerosol/Gas	Solid	<i>Form dew, Condense into alcohol</i>
	Vaporize	Liquid	Aerosol/Gas	<i>Humidifier sprays water, Boil water</i>
	Crystallize	Liquid	Solid	<i>Making salt, Making sugar</i>
	Sublimate	Solid	Aerosol/Gas	<i>Burn coal, Burn plastic</i>
	Dissolve	Solid	Liquid	<i>Dissolve the tablet, Make formula</i>
	Compress	Solid	Liquid	<i>Juicing fruits, Extracting pomegranate juice</i>
	Flow out	Solid	Non-Viscous	<i>Break chocolate with a liquid center</i>
	Soften	Solid	Viscous	<i>Boil sugar, Bake cheese</i>

our dataset pipeline efficiently declines the model bias of annotations.

12.1. IoU Analysis

In terms of model selection of the dual-model cross-validation process, we adapt the annotation model to the latest SAM2 [25]. We utilized the open-source base plus model configuration and checkpoints, as this configuration is more effective in fully segmentation [9, 25, 32] of our target objects compared to other model setups.

In the dual-model cross-validation, we first randomly sampled a subset of videos annotated by Cutie at a ratio of 5:1. We selected 6 volunteers from a total of 12 to re-annotate this subset using both the SAM2-assisted and Cutie-assisted annotation tools, resulting in masks designated as Mask A and Mask B, respectively. To balance annotation efficiency and validation effectiveness, we set the annotation frame rate to 6 fps in the cross-validation. The

high-frame-rate annotated masks obtained for the dataset are referred to as Mask O.

By calculating the Intersection over Union (IoU) and the other two metrics introduced in [29, 34], the results are shown in Fig. 7, indicated that J_{st} (MaskA, MaskB) and J_{mean} exceeded 85% and were very close to each other. Specifically, although the difference between Mask A and Mask B is slightly larger than that between Mask B and Mask O, we have Eq. (4) holds:

$$\mathcal{J}_\sigma(B, O) - \mathcal{J}_\sigma(A, O) \ll 1 - \mathcal{J}_\sigma(B, O). \quad (4)$$

These results suggest that the annotations SAM2-assisted annotation tool produced are comparable to those of the Cutie-assisted tool, without significant bias due to model differences. They also indicate that the bias introduced by the models can be considered negligible compared to other sources of systematic error, such as volunteer annotation habits and inadvertent jitters during annotation.

Table 9. The detail of the definition of different phase transitions.

Category	Phase Transition	Definition
Intra-Phase (Solid)	Separate	Block-like solid objects are disassembled into multiple block-like pieces
	Twist	Flexible objects are deformed into various shapes.
	Break	Solid objects are shattered into countless small fragments.
	Stretch	Flexible objects are elongated into a longer form.
	Split	The solid particles disperse in all directions, spreading out from the source.
	Merge	Multiple block-like objects are combined into a single whole.
	Crush	Solid block-like objects are ground into powdery granules.
Intra-Phase (Liquid)	Flow	The liquid moves as a whole under the influence of external force.
	Paint	The liquid is applied onto a solid surface.
	Splash	The liquid is scattered in all directions due to a sudden external force.
	Mix	One liquid is poured into another, causing the two liquids to blend together.
	Drip	A small amount of liquid is transferred drop by drop.
Intra-Phase (Aerosol/Gas)	Diffuse	The gas or aerosol spreads out, gradually expanding its presence in the air.
Cross-Phase	Solidify	The liquid turns into a solid as it cools or hardens.
	Melt	The solid turns into a highly fluid liquid.
	Deposition	The gas directly transforms into a solid without passing through the liquid state.
	Vaporize	The liquid turns into a gas as it heats up and evaporates.
	Crystallize	The solid crystals form and separate out from the liquid.
	Sublimate	The solid directly produces gas as it transitions without becoming a liquid.
	Dissolve	The substance disperses evenly in the liquid, forming a solution.
	Compress	The solid is squeezed under pressure, forcing a large amount of liquid to be released.
	Flow out	The liquid content flows out from within the solid as it is released or displaced.
	Soften	The solid gradually turns into a thick, viscous liquid.

12.2. Blind Review: DMOS Evaluation

In addition to the quantitative analysis of model bias conducted using the dual-model validation, we also designed a mechanism for blind comparison by experienced reviewers. We presented 3 reviewers with both Mask A and Mask B from the cross-validation annotation process, allowing them to evaluate the performance of the two masks based on the three criteria mentioned in Sec. 11.1. The reviewers were instructed to select the mask they deemed superior. If they considered the performances to be equivalent, they could choose *Equal*. Throughout this process, the order of Mask A and Mask B was randomized to ensure that the reviewers were unaware of which mask corresponded to which model.

The final subjective evaluation results are shown in Fig. 8, indicating that the two masks demonstrated a considerable degree of consistency across the three subjective evaluation metrics, with no significant bias observed.

13. Multi-Level Semi-Auto Annotation Tool

In Fig. 9, we show our details of the interactive UI of the multi-level semi-auto annotate tool. We implement this tool based on the interactive demo from Cutie [4], including pixel level, appearance level, and object level. In particular, we implement the object-level function using the SAM2 model and Cutie model. In this way, we could perform the dual-model cross-validate analysis in Sec. 12.

14. Details of Core Subset

We extract a subset of cases that better represent the full dataset and refer to it as a core subset. For each specific scenario, we extracted a subset of cases. During the selection of the core subset in each scenario, we consider a series of factors: the number of the full set, the number of classes included, and the difficulty of cases. As is shown in Tab. 10, We choose the size of the core subset of each scenario to

Table 10. Details of core subset number of different Scenarios

Scenario	Full Set Number	Core Subset Number	Class Number	Example
Factory	67	9	13	<i>Disassemble/assemble a gun, Wrap a wire</i>
Handicraft	40	12	14	<i>Knit a sweater, Wrap a cigar</i>
Kitchen	163	12	70	<i>Cut celery, Shave fish</i>
Lab	152	12	56	<i>Drip liquid, Dissolve drug</i>
Housework	3	3	2	<i>Twist mop</i>
Decoration	9	2	2	<i>Tear wallpaper</i>
Hospital	7	2	4	<i>Ground herbal</i>
School	1	1	1	<i>Sharpen a pencil</i>
Farm	13	3	7	<i>Shear a sheep</i>
Sport	2	1	1	<i>Hit a balloon</i>
Daily live	45	14	18	<i>Pour tea, Shave beard</i>
Experiment field	14	6	3	<i>Pour tea, Shave beard</i>

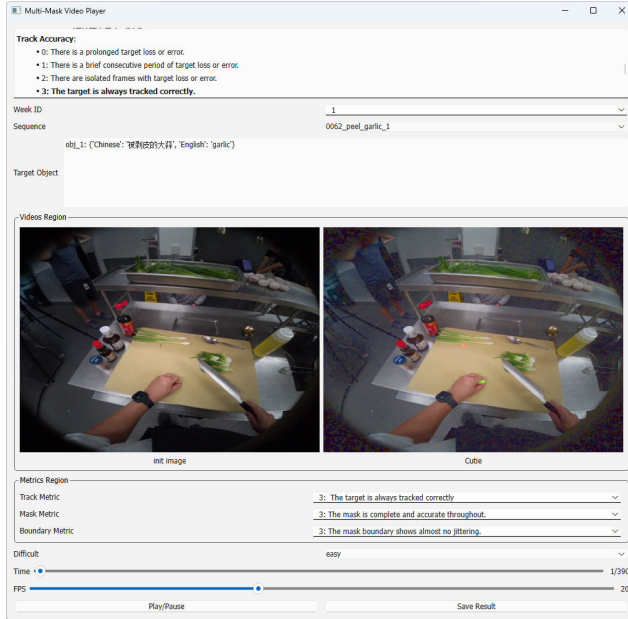


Figure 6. Review UI. The reviewer is required to evaluate the mask annotation from three criteria.

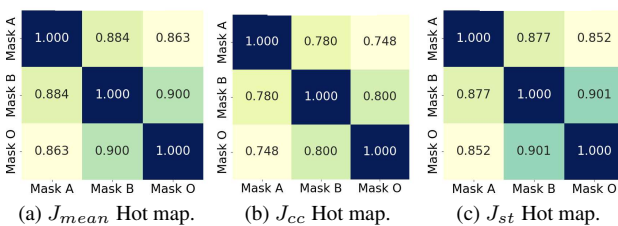


Figure 7. IOU Analysis among Mask A (SAM2), Mask B (Cutie Dual), and Mask O (Cutie in the final dataset).

make it closer to the proportion of the full set and the class number.

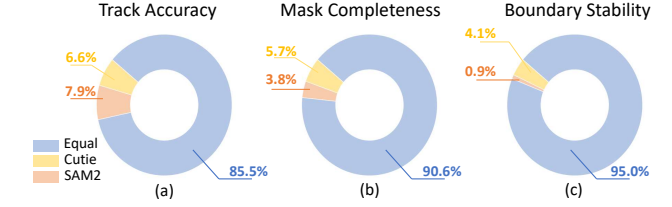


Figure 8. The result of blind review. Through subjective evaluation of three metrics (a) Track Accuracy, (b) Mask Completeness, and (c) Boundary Stability, we found that the Mask results obtained with Cutie-assisted annotation and SAM2-assisted annotation show little difference in performance.

15. Challenge Analysis

In this part, we explore how the size of the object and the velocity of the target object influence the performance of Cutie-ReVOS.

15.1. Definition of Object Size

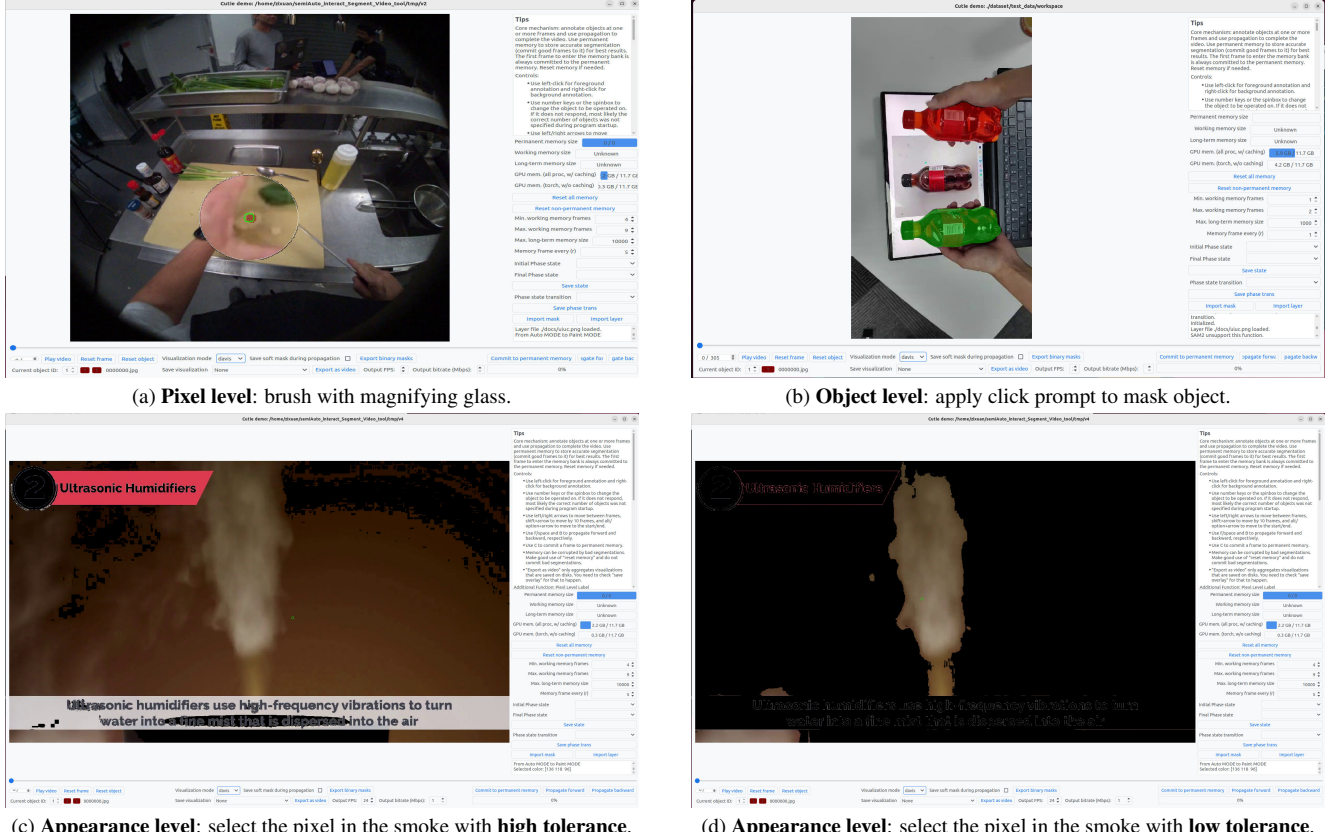
In our experiment, given a target object o in the image I , its size is measured by the ratio between the mask of the object M_o and the area of the image A_I , according to

$$R(o) = \frac{M_o}{A_I}, \quad (5)$$

where $R(o)$ measures the relative size of the object compared to the Image. M_o is the size of the ground-truth mask of the object O . A_I is the area of Image I .

15.2. Definition of Velocity

Generally, the velocity of an object in an image is defined as the change in the centroid of the bounding box or mask per unit time. However, considering that we cannot measure the relationship between the distance in the image and the actual size of the object, we normalize the velocity based on the size of the object. Given a target object o and the fps



(c) Appearance level: select the pixel in the smoke with **high tolerance**.
 (d) Appearance level: select the pixel in the smoke with **low tolerance**.

Figure 9. Multi-level semi-auto annotate tool: our annotate tool implements three-level annotating (**pixel level**, **appearance level**, **object level**). Using this tool, we can efficiently annotate different objects, such as small objects *garlic* in (a), solid with clear boundaries *cola bottle* in (b) and fluid object *smoke* in (c), (d).

f_v of the video clip, the relative velocity or the normalized velocity is defined as follows:

$$v(o) = \frac{D(o)f_v}{M_o}, \quad (6)$$

$$D(o) = c_t(B_o) - c_{t-1}(B_o),$$

where B_o is the bounding box of target object o . $c_t(B)$ is the centroid of the bounding box in the timestamp t . $D(o)$ is the moving distance of the Object in a frame.

15.3. Relation between Challenge and Performance

As the curve in Fig. 10a demonstrated, the smaller the object's area ratio, the more challenging it is for the model to segment. Besides, for small objects, the performance of ReVOS-Cutie decreases compared to the original Cutie. For large objects, the situation is reversed.

Similarly, the curve in Fig. 10b indicates that the relative velocity positively correlates with segmentation difficulty. We observe that when the velocity is more extreme, either too slow or too fast, the performance improvement of ReVOS-Cutie becomes more significant.

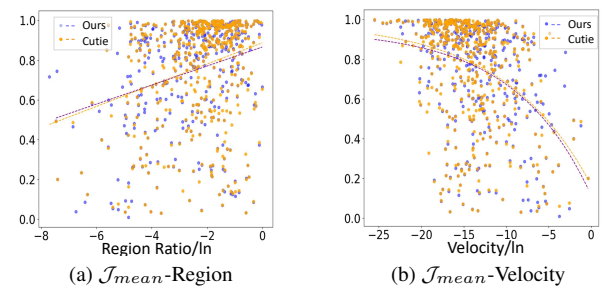


Figure 10. The relation between standard metric Jaccard index J_{mean} and region size, velocity.

16. More Failure Cases

In this part, we show more failure cases of the current models in Figs. 11 and 12.

In case 1 (*fry dough*) of Fig. 11, the boiling oil makes it difficult to separate the boundaries of the dough sticks accurately. Even for some models, the boiling oil causes the tracking loss. However, our method improves the segment accuracy with visual distribution.

In case 2 (*assemble puzzles*) of Fig. 11, the intra-solid

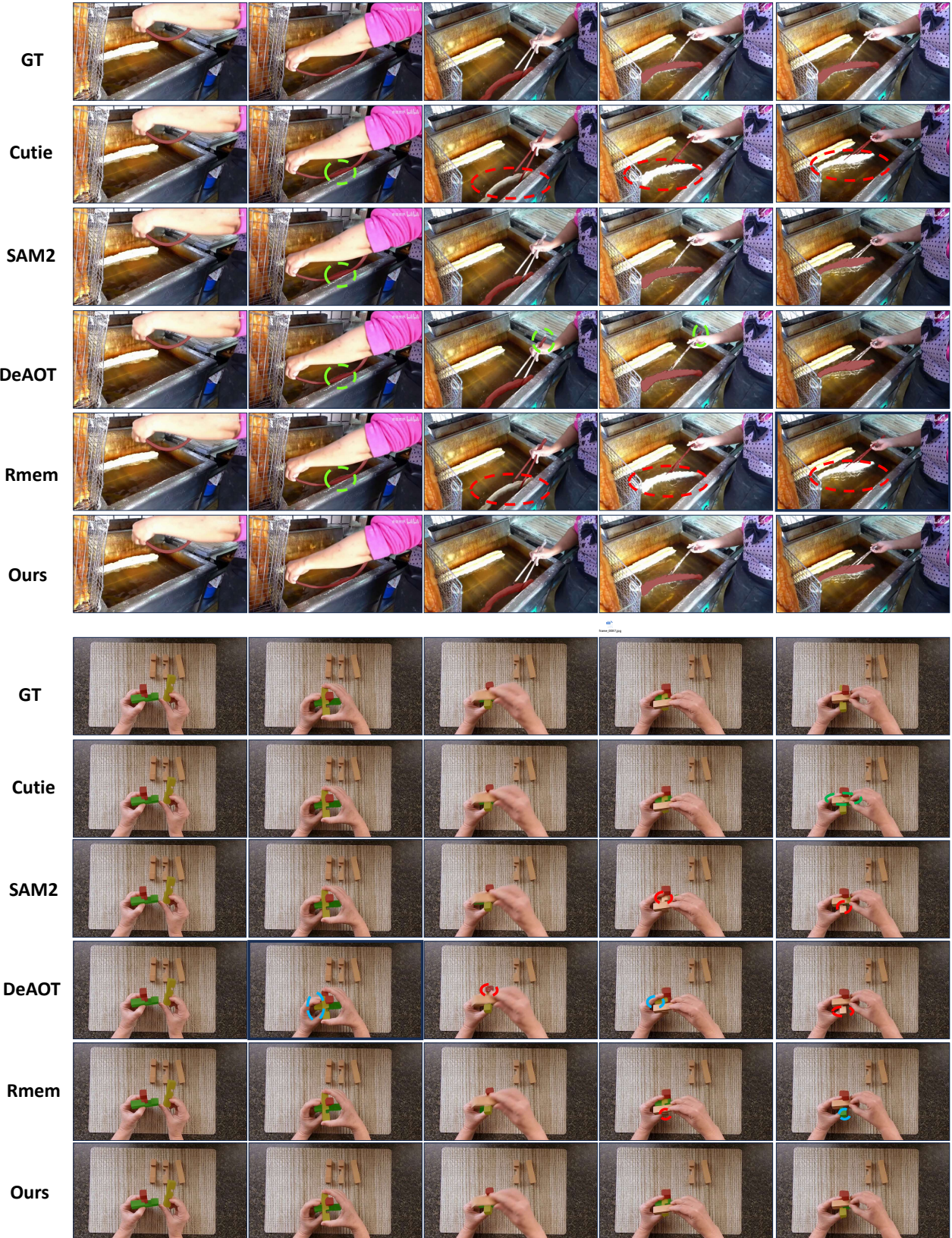


Figure 11. Failure case 3 (*fry dough*) and 4 (*assemble puzzles*) in different models. (Red circle: false-negative region; Green circle: false-positive region; Blue circle: confuse-instance region).

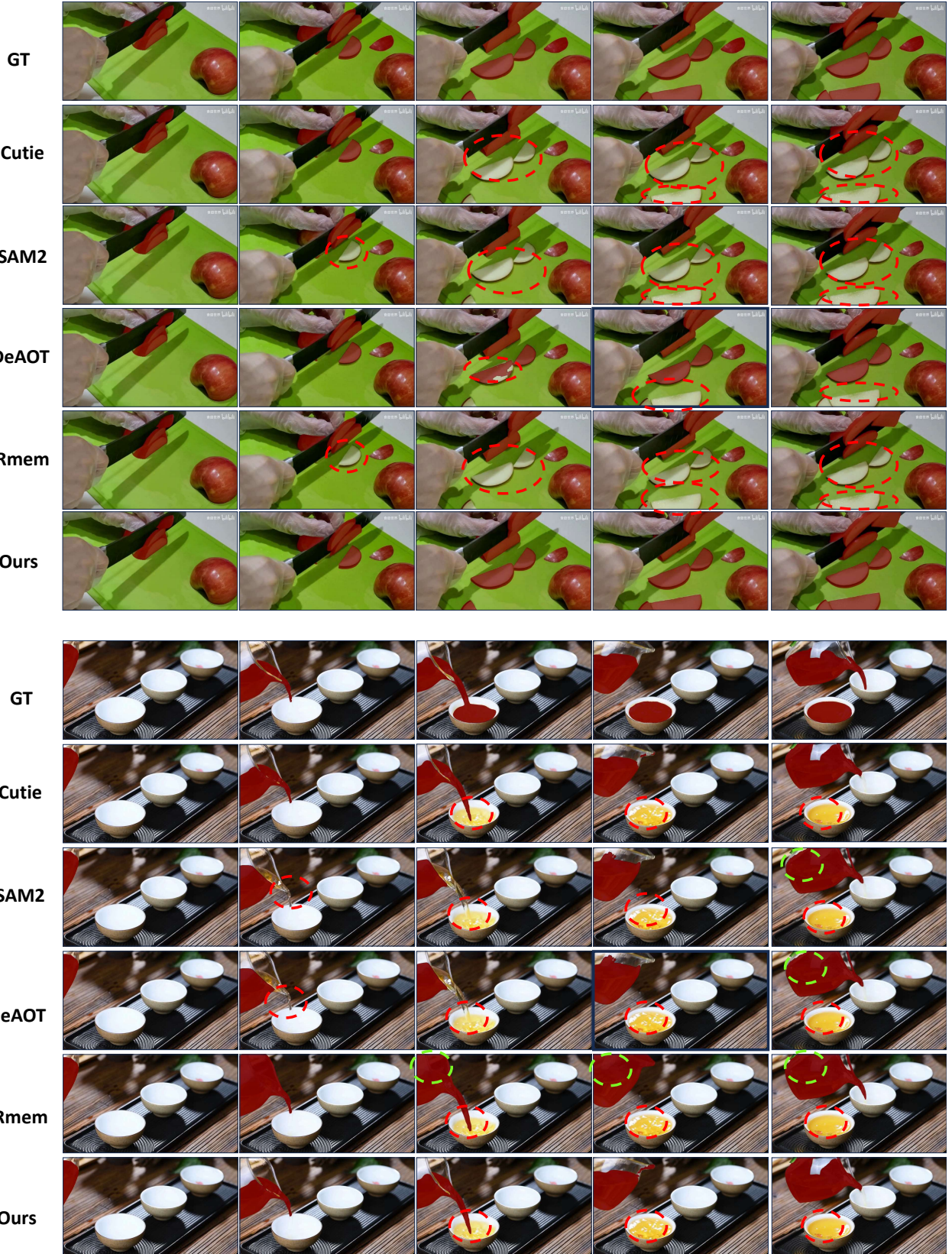


Figure 12. Failure case 1 (*cut apples*) and 2 (*pour tea*) in different models. (Red circle: false-negative region; Green circle: false-positive region).

transition with multi-instances usually instance confusion because of the similarity distribution. However, our methods are more robust when facing the intra-solid transition with multi-instances.

In case 1 (*cut apples*) of Fig. 12, the tracking loss and mask incompleteness usually happen when the white pulp leaks out. The performance in the intra-solid phase transition with the color change challenge is not so good.

In case 2 (*pour tea*) of Fig. 12, the flow of tea liquid into the tea cup is always accompanied by tracking loss. Besides, transparent teapots and tea liquids are confused and suffer from similar interference. Although our method improves this situation slightly, this multi-challenge case still has improved space.